JACS
JOURNAL OF THE AMERICAN CHEMICAL SOCIETY

Article

pubs.acs.org/JACS

New Insights into Electronic and Geometric Effects in the Enhanced Photoelectrooxidation of Ethanol Using ZnO Nanorod/Ultrathin Au Nanowire Hybrids

Annamalai Leelavathi,[†] Giridhar Madras,[‡] and Narayanan Ravishankar*[,§]

[†]Centre for Nanoscience and Engineering, [‡]Department of Chemical Engineering, and [§]Materials Research Centre, Indian Institute of Science, Bangalore-560012, India

Supporting Information

ABSTRACT: Oxidation of small organic molecules in a fuel cell is a viable method for energy production. However, the key issue is the development of suitable catalysts that exhibit high efficiencies and remain stable during operation. Here, we demonstrate that amine-modified ZnO nanorods on which ultrathin Au nanowires are grown act as an excellent catalyst for the oxidation of ethanol. We show that the modification of the ZnO nanorods with oleylamine not only modifies the electronic structure favorably but also serves to anchor the Au nanowires on the nanorods. The adsorption of OH^- species on the Au nanowires that is essential for ethanol oxidation is facilitated at much lower potentials as compared to bare Au nanowires leading to high activity. While ZnO shows negligible electrocatalytic activity under normal conditions, there is significant enhancement in the activity under light irradiation. We demonstrate a synergistic enhancement in the photoelectrocatalytic activity of the ZnO/Au nanowire hybrid and provide mechanistic explanation for this enhancement based on both electronic as well as geometric effects. The principles developed are applicable for tuning the properties of other metal/semiconductor hybrids with potentially interesting applications beyond the fuel cell application demonstrated here.

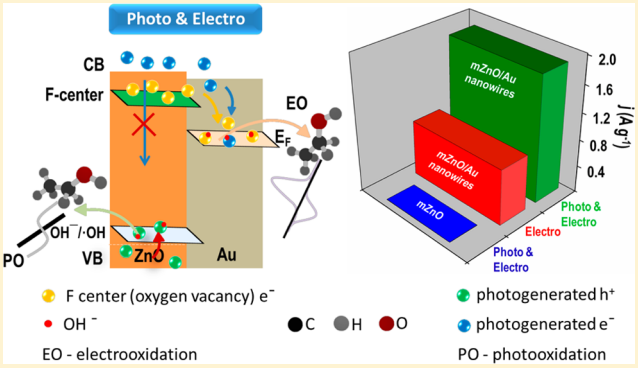

INTRODUCTION

Rising energy demands and the depletion of nonrenewable resources have motivated research and development of liquid fuel cells. Particularly, efforts have been geared toward the oxidation of small organic molecules (SOM) that are recognized as the richest source of fuels. Among the SOM, ethanol has considerable advantages in terms of its high energy capacity, no toxicity and possibility of deriving it from biomass.[1,2] Nevertheless, direct ethanol fuel cells (DEFC) have limitations for anode materials owing to complex reactions that involve breaking of C−C bonds.[3] Traditionally Pt-based anodes have been shown to exhibit high efficiency toward alcohol oxidation; however, they suffer from the reaction intermediate CO poisoning during operation.[4] Numerous studies have focused on engineering Pt-free nanostructured catalysts for improved durability and enhancement in electrochemical activity.[5−7]

Ultrathin nanowires are attractive as electrocatalysts because of their inherent dimensional confinement.[8−11] Au nanowires have been shown to adopt exotic structures[12] with enhanced chemical reactivity toward oxidation reactions.[13] For instance, Au nanowires displayed negative shift in the redox potential of ferri/ferrocyto-c relative to Au thin films.[14] Wet chemical reduction with oleylamine as both the reducing agent as well as the capping agent is a promising method for high yield synthesis of Au nanowires for applications.[15] However, the inherently low stability of these nanowires precludes harsh cleaning treatments and hence limits their application.[14] The capping agent on the Au nanowires may also modify the surface properties and possibly hinder the electron transfer during electrocatalytic reactions and thus slow down the rates.[14] A possible way to overcome the aforementioned issues is to anchor the wires on a specific support that increases the stability of the wires in polar medium and also provides flexibility to remove undesired surfactants.[16] While there are a few methods available to anchor nanowires on substrates,[17−19] there is no general method that may be applicable for a variety of substrates because the nanowires grow via a nonclassical oriented attachment process.[20,21]

Among all the possible support materials, the distinct property of metal oxide semiconductors makes them an ideal platform to anchor electroactive materials with potential enhancement in multifunctionality.[22] The possibility of minimizing CO poisoning via bifunctional mechanism by transfer of lattice oxygen[23] and an enhancement of electrocatalytic activity via photoexcitation are two attractive features associated with semiconducting oxide supports.[24−27] Consid-

Received: June 13, 2014
Published: September 22, 2014

   dx.doi.org/10.1021/ja5059444 | J. Am. Chem. Soc. 2014, 136, 14445−14455

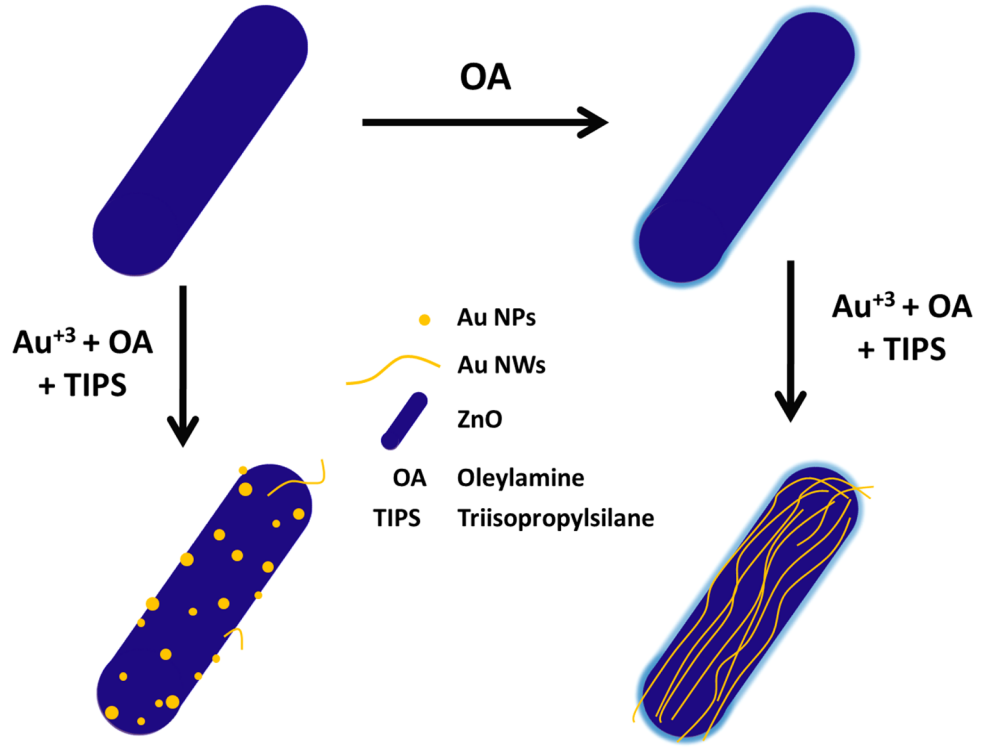

Figure 1. Schematic illustration of the procedure to synthesize ZnO/Au nanowire hybrids. Conventional method to grow ultrathin Au nanowires on ZnO leads to the formation of particles with a very few wires. Modification of ZnO with oleylamine aids in the growth of nanowires.

erable progress has been achieved to synergistically enhance the electrochemical properties for exciting photofuel cell applications.[28] Among the large family of photoactive materials, ZnO has been extensively investigated because of its outstanding electron mobility that results in high photoactivity besides low material cost and nontoxicity. Specific geometries of the crystal facets exhibit different photocatalytic activities and thus there have been significant efforts to design the morphology of nanomaterials.[29] In particular, high aspect ratio 1D nanostructure retains the advantages of superior photogenerated carrier transport with low rate of recombination.[30] Furthermore, it was found that the separation efficiency of photogenerated charge carriers was enhanced by post-treatment of metal oxides surfaces with either organic[31] or inorganic ligands[32,33] that results in the elimination of midtrap states.

Based on the above considerations, we have developed a simple in situ strategy to grow ultrathin Au nanowires on oleylamine (OA) passivated ZnO nanorods (designated as mZnO) for electrocatalytic oxidation of ethanol. The strong grafting of ZnO with OA is the key for providing Au nucleation sites, followed by subsequent growth of nanowires through oriented attachment mechanism. In this study, the insight gained through cyclic voltammetry (CV) measurements leads to useful information about versatile role of ZnO; mZnO not only serves as support to stabilize the ultrathin nanowires against disintegration in ethanol fuel cells while in operation but also promotes the electrocatalytic activity via electronic effect. This effect is related with electron donation to Au nanowires from ZnO that determines the formation of incipient hydrous gold oxides at low potential. These oxide species serve as redox mediators for electrocatalytic oxidation of ethanol at low potential; repeated high potential cycling is needed to promote the oxidation reaction in the case of bare Au nanowires. We also demonstrate a significant increase in the electrochemical activity via photoexcitation. Our experimental study demonstrates that ultrathin nanowires are potentially interesting systems for catalysis applications provided they are stabilized by a suitable support. In the present case, the support, in addition to providing stability, also promotes the activity of Au nanowires at lower potential in addition to imparting significant improvement in activity in the presence of light. We discuss the origin of this synergistic enhancement that provides key insights into the development of multifunctional hybrids with potential solutions for energy and environment-related issues.

RESULTS AND DISCUSSION

Passivation of ZnO by Oleylamine: Implications for Hybrid Formation and Properties. A schematic illustration of the methodology employed for the preparation of ZnO/Au nanowire hybrid is shown in Figure 1 and involves the modification of ZnO by oleylamine (OA) followed by the growth of ultrathin Au nanowires on mZnO. High aspect ratio ZnO (1 μm length) was initially prepared according to our earlier report.[30] ZnO nanorods were mixed with oleylamine (OA) using a mortar and pestle. The mixture was finally washed with hexane and ethanol mixture to remove the excess unbound amine. The amine groups bound to the surface of ZnO facilitate the growth of Au nanowire on the ZnO nanorods.[34] This is evident from the experiments carried out without surface modification that resulted in very few ultrathin nanowires on support and primarily leads to the formation of larger size Au nanoparticles in both solution as well as the support (Figure S1, Supporting Information). In our earlier report, we had shown that Au nanowires can be grown on metal oxide but the areal density of nanowires was very much limited, which hampers potential applications.[35] Our modified scheme of passivating the ZnO by direct mixing of the

dx.doi.org/10.1021/ja5059444 | J. Am. Chem. Soc. 2014, 136, 14445−14455

nanorods with OA rather than dispersing the rods in a solvent containing OA clearly results in much better binding of the amine on the ZnO surface and is responsible for the growth of high areal density ultrathin Au nanowire on ZnO. Solid state mixing resulted in higher concentration of OA immobilized on ZnO with respect to mixing in hexane solvent (Figure S2).

The high angle annular dark field (HAADF) image (Figure 2A) reveals a uniform distribution of ultrathin Au wires on mZnO. Bright-field TEM images show that, in some instances, the grown Au nanowires are aligned along the entire length of the nanorods to form longitudinal bands (Figure S3). The higher magnification HAADF image (Figure 2B) suggests that nanowires are well separated; the distance of separation is approximately equal to OA chain length (2 nm).

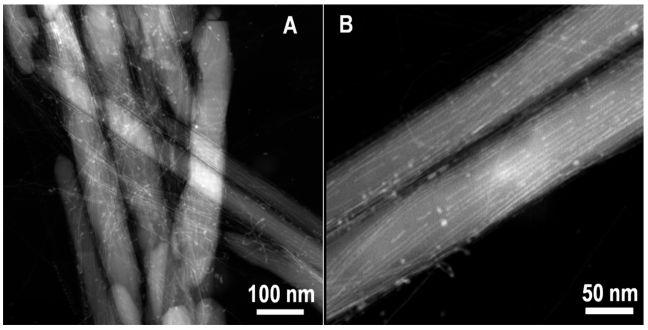

Figure 2. STEM-HAADF images of as-synthesized mZnO/Au nanowires. (A) Image displaying dense growth of ultrathin wires on mZnO and (B) higher magnification image showing wires aligned parallel to the long axis of the nanorods.

The binding of amine to the surface of ZnO has been verified using X-ray photoelectron spectroscopy (XPS) and Fourier transform infrared (FT-IR) spectroscopy. High resolution N 1s spectra of mZnO can be deconvoluted into two peaks as shown in Figure 3A, peaks at 398.8 and 400.2 eV which are assigned to nitrogen atom in oleylamine and oleylammonium cation.[36] This strongly suggests the adsorption of nitrogen species on ZnO surface. The deconvoluted oxygen spectra confirm the existence of oxygen defects (Figure S4). Figure S5 (Supporting Information) represents the FTIR spectra of ZnO and mZnO, which shows the existence of amine species after modification. The N−H stretching vibration of OA was merged with O−H vibration. The bands observed at 2923 and 2853 cm^{-1} are attributed to C−H antisymmetric and symmetric stretching vibration of CH_2, respectively.[37] In mZnO, we observed strong absorption at 1064 cm^{-1} corresponding to shifted C−N bands of OA emphasizing that OA is grafted on surface of ZnO.[15] In addition, we see drastic variations in the density of states after OA modification on ZnO as seen in the UPS valence spectra (Figure S6).

To examine the electronic interaction of OA with ZnO nanorods, we measured current before and after modification of ZnO. Previous studies have shown that amine grafting on ZnO can modulate the electrical conductivity that was explained on the basis of the dipolar fields offered by the amine groups.[38] In contrast, *I*−*V* measurements in our present work displayed negligible change in the conductivity after OA modification (Figure S7). However, in the presence of light, we observed a 2-

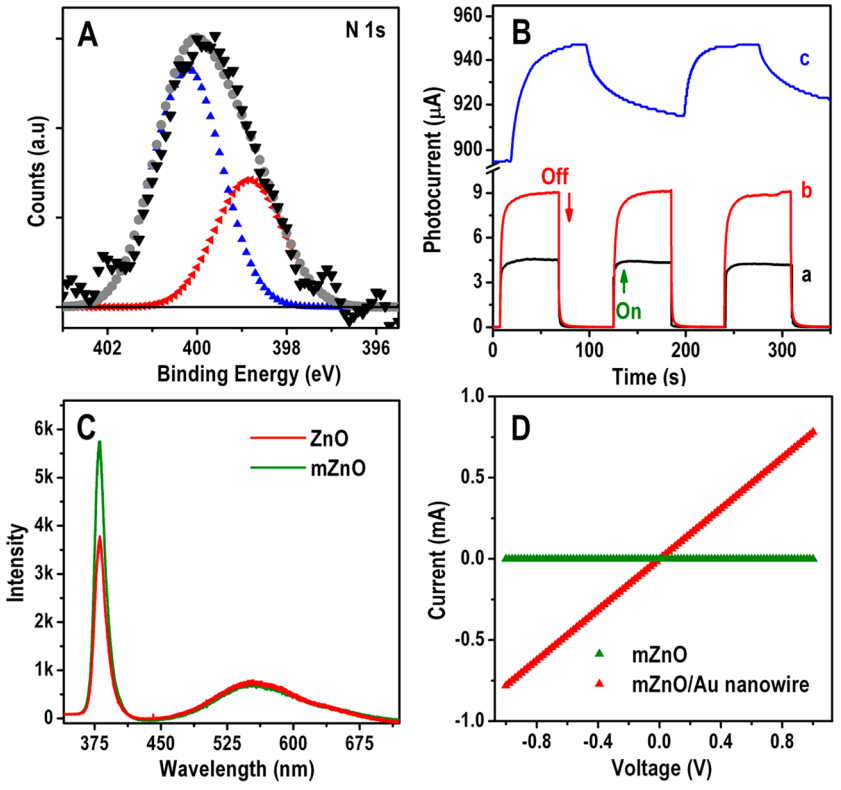

Figure 3. (A) Deconvoluted N 1s XPS spectrum of amine-modified ZnO (mZnO), displaying the existence of nitrogen species. (B) Photocurrent of ZnO (a), mZnO (b), and mZnO/Au (c) nanowires upon solar light (xenon lamp) illumination. (C) Photoluminescence spectra (PL) of ZnO and oleylamine-modified ZnO. Oleylamine modification results in marked enhancement of band-edge emission peak (excited at 325 nm). (D) Current−voltage characteristic of mZnO and mZnO/Au nanowire hybrid measured in ambient, showing enhanced electrical conductivity of the hybrid.

dx.doi.org/10.1021/ja5059444 | J. Am. Chem. Soc. 2014, 136, 14445−14455

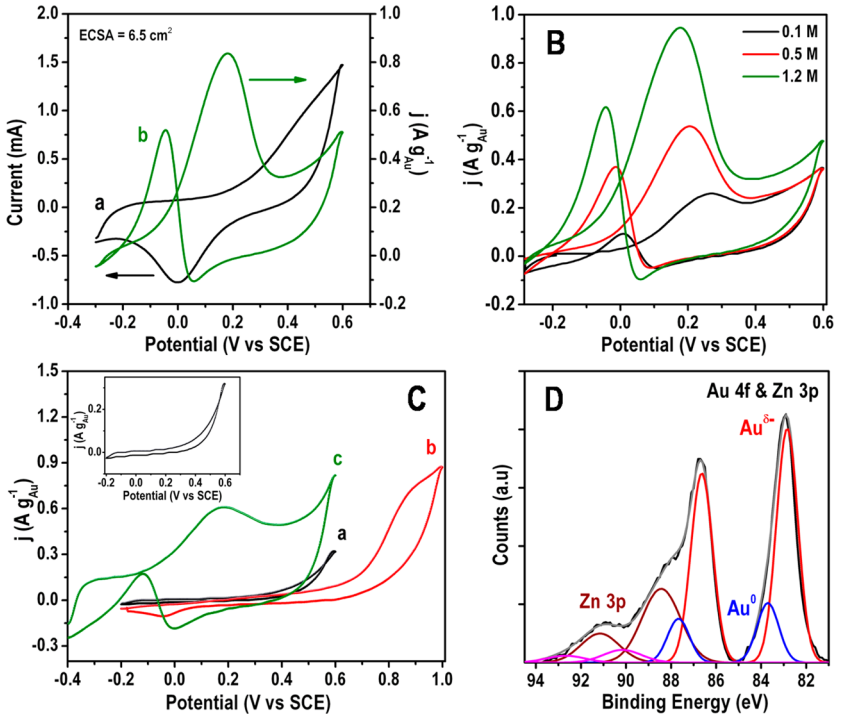

Figure 4. Cyclic voltammograms (CV) of mZnO/Au nanowires. (A) (a) 1 M NaOH (without ethanol); the electrochemical surface area was calculated from the backward reduction peak area (from −0.2 to 0.2 V vs SCE) (for 0.06 mg) and (b) with 1.5 M ethanol in 1 M NaOH showing characteristic oxidation peak of ethanol. (B) CV with different molar concentration of NaOH containing 1.5 M ethanol. (C) CVs of bare ultrathin Au nanowires in 1 M NaOH containing 1.5 M ethanol with different positive potential limits. (a) Cycling up to 0.6 V (enlarged in the inset) showing featureless voltammogram. (b) Characteristic oxidation and reduction peak of Au appeared after cycling to 1 V. (c) Ethanol oxidation peak is observed in the next cycle after initial cycling to 1 V. All the scan rates are at 40 mV/s. (D) Deconvoluted XPS Au 4f spectra of mZnO/Au nanowires showing the existence of Au anionic species.

fold increase in the generated photocurrent from mZnO with an applied voltage of 0.5 V as shown in Figure 3B. Photoluminescence studies were performed to investigate the impact of OA on observed photoresponse. We note that OA modification significantly increased the UV band edge emission of ZnO (by ∼1.5 times) as shown in Figure 3C, thus confirms an electronic interaction of the amine with ZnO. This suggests that the nonradiative emission associated with uncoordinated bonds is effectively removed which is consistent with the intensified band-edge emission.[39] However, the visible emission remains almost same. In principle, visible emission originates from defect states, serves as scavenger, and facilitates the separation of photogenerated charge carriers, consequently increasing the carrier lifetimes.[40] As the degree of passivation increases with increase in the concentration of OA relative to ZnO, an increase in the photocurrent was observed consistent with the proposal that amine interacts strongly with the ZnO surface (Figure S8). By decreasing the OA concentration, the band edge emission decreases as shown in Figure S9.

Although, ligand-passivated ZnO has been investigated earlier,[41,39] our results differ from many of the existing observations in the following ways. First, the passivation is seen to affect only the nonradiative recombination and accounts for the best possible separation of photogenerated charge carriers. Second, the passivation preserves the electronic defect states that are responsible for suppressing the recombination of carriers. In addition to these electronic effects, the passivation presents strong anchoring sites for the nucleation of Au nanoparticles that subsequently assist in the growth of ultrathin wires. Furthermore, ultrathin Au nanowires grown on mZnO displayed excellent electrical conductivity[42,43] (Figure 3D), signifying that high aspect ratio ultrathin Au nanowire can, in principle, be used for electrocatalytic applications. The hybrids exhibit a further sharp increase in photocurrent, revealing that the photoexcited electron can possibly transfer from ZnO to Au nanowire leading to a better separation of the photogenerated charge carriers.[44] Although nanowires utilized in this study absorb across a range of visible light wavelength (Figure S10), we do not observe any measurable photocurrent generation by bare nanowires as shown in Figure S11. This is also validated by the wavelength-dependent photocurrent measurements on mZnO/Au as depicted in Figure S12. These results highlight that surface modification of ZnO either with suitable passivation groups and/or metal nanostructures is a viable method to enhance the electro- and photoconductivity.

Electrocatalysis Using mZnO/Au Nanowires. Inspired by the photo and electrical properties of mZnO/Au nanowires, we investigated them as possible photoassisted electrocatalysts for alcohol oxidation reactions. To gain insights into the photoelectrocatalytic activity, we first studied the ethanol oxidation (EOX) on mZnO/Au (without light) in alkaline medium in order to evaluate the electrocatalytic activity of the electrode. The electrochemical surface area (ECSA) of the electrode was measured using cyclic voltammetry (CV) in 1 M NaOH electrolyte solution without ethanol at a scan rate of 40 mV/s (Figure 4A). During forward scan, the slight increase in the current at very low potential is attributed to the charge transfer process associated with OH^- group adsorption (reaction 1, below) that plays a key role in alcohol oxidation.

dx.doi.org/10.1021/ja5059444 | J. Am. Chem. Soc. 2014, 136, 14445−14455

The characteristic peak for monolayer oxide formation on Au takes place during the forward scan.[45] The cathodic peaks observed during the reverse scan correspond to the reduction of Au oxide and to the desorption of hydroxyl groups.[16] The electrochemical actual surface area (ECSA) was estimated by a calculation of the oxide reduction peak area from the CV scans. The oxidation current was normalized to ECSA for the respective electrodes for further comparison of the catalyst activities (Supporting Information), current density obtained for nanowire hybrid is higher when compared to polycrystalline Au electrode.[46,47] The obtained oxidation current was normalized with mass of the gold to calculate current density. The voltammetric response in the presence of ethanol (1.5 M of CH_3CH_2OH in 1 M NaOH) for synthesized mZnO/Au shows that the beginning of the EOX reaction coincides with the chemisorption of OH^- process; current density increases at very slow rate below 0 V and with increasing potential the current increases indicating the initiation of EOX (Figure 4A). At 0.18 V, the oxidation current reaches a maximum and then decreases with further increasing potential, which can be attributed to the formation of an inactive compact oxide layer on Au surface. In the reverse scan, the peak appeared at −0.05 V corresponds to the removal of incompletely oxidized carbonate species absorbed on the gold surface. This peak onset potential coincides with reduction peak of gold in the ethanol-free NaOH solution, which can be attributed to the reactivation of the Au surface.[47]

The oxidation of alcohols in the alkaline medium occurs only when the gold electrode surface is partially covered with oxygenated species. Several studies have indicated that alcohol oxidation reactions take place even on gold surfaces that do not have significant chemisorbing capacity only if an interfacial cyclic redox mediator forms during the reaction as exemplified by the incipient hydrous oxide/adatom mediator model.[48] The driving force for the formation of such species is more favorable in alkaline medium through adsorption of OH^-,[46] and the oxidation reaction has been suggested to follow the steps shown below. It is well-documented that C_2 is the preferred pathway for EOX on gold; the initial step in this case involves the formation of aldehyde.[46]

$$\mathrm{Au} + \mathrm{OH}^- \rightarrow \mathrm{Au} - (\mathrm{OH})_{\mathrm{ads}}^{(1-\lambda)-} + \lambda \mathrm{e}^- \quad (1)$$

$$\mathrm{CH_3CH_2OH} + \mathrm{OH}^- \rightarrow \mathrm{CH_3CH_2O} + \mathrm{H_2O} + \mathrm{e}^- \quad (2)$$

$$\mathrm{CH_3CH_2O} + \mathrm{Au(OH)_{ads}} \rightarrow \mathrm{Au(CH_3CHO)} + \mathrm{H_2O} + \mathrm{e}^- \quad (3)$$

$$\mathrm{Au(OH)_{ads}} + \mathrm{CH_3CHO} + \mathrm{OH}^- \rightarrow \mathrm{Au} + \mathrm{CH_3COOH} + \mathrm{H_2O} + \mathrm{e}^- \quad (4)$$

The chemisorption of hydroxyl groups will be favored on the gold surface that leads to partial oxidation of gold (reaction 1). The first deprotonation of ethanol is base catalyzed (reaction 2),[47] and hence, the formation of alkoxide will be enhanced with increasing concentration of NaOH. In fact, the second hydrogen elimination from alkoxide involves an OH^- adsorbed Au surface; this dehydrogenation step leads to aldehyde formation.[49] The aldehyde further reacts with OH^- to produce acetic acid. Almost all the above steps are greatly influenced by OH^- ions either in solution (reaction 2) or chemisorbed on the Au surface (reaction 3 and 4).[50,51] As expected from the above reactions, an increase in the concentration of NaOH, the oxidation peak shifted negatively that unambiguously confirms that hydroxyl adsorption has a promoting effect on EOX (Figure 4B).

The measured electrocatalytic activity of mZnO/Au nanowires for EOX was compared with the activity of unsupported nanowires. Scanning and transmission electron microscopy (SEM and TEM, respectively) micrographs of the unsupported OA capped Au nanowires are shown in Figure 5A and B. The

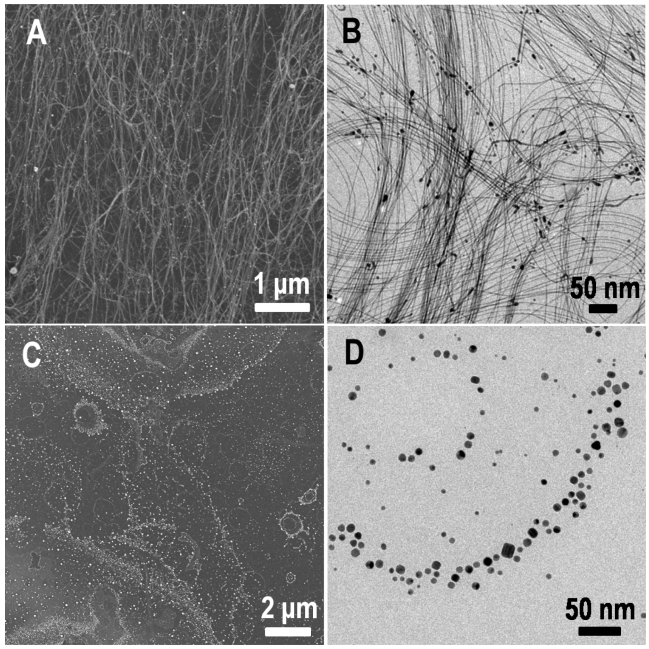

Figure 5. SEM and TEM bright field images of unsupported ultrathin Au nanowires (A,B) before and (C,D) after EOX reaction. Unsupported nanowires are not stable, indicating that the nanowires disintegrate and aggregate to form nanoparticles during reaction.

electrocatalytic oxidation current was negligible in the case of bare Au nanowires (curve a, Figure 4C) under similar conditions as those used for mZnO/Au. It has been shown that the presence of an amine capping layer on the Au can lead to suppression of redox processes, resulting in a featureless voltammogram.[14] We observe that when the potential is swept to higher values (above 0.6 V), an anodic oxidation feature was observed around 0.9 V attributed to the formation of oxide species on gold surface accompanied by a reversible reduction of formed oxide layer observed at −0.05 V in negative scan (as shown in Figure 4C, curve b). For the subsequent scans, intriguing changes are observed as suggested by the appearance of the sharp quasi-coincidence of forward and reverse anodic oxidation features at 0.18 V and −0.1 V and can be ascribed to the oxidation of ethanol and the formed intermediates respectively (Figure 4C, curve c). These results suggest that scanning at higher potential is observed to have a significant influence on the formation of Au oxygenated mediators and that these formed products promote redox reactions, resulting in the oxidation of ethanol in the following cycles.

Although the exact mechanism is not known, we hypothesize that OA capping on nanowires masks the formation of Au oxygen mediators at low potential. It has been proposed that the amine can form a complex with Au with applied potential in basic solution and that the complex formed at the interface can retard the formation of oxygenated gold species.[48] Scanning to

dx.doi.org/10.1021/ja5059444 | J. Am. Chem. Soc. 2014, 136, 14445−14455

Scheme 1. Charge Transfer Scenarios between ZnO and Au Nanowires during (A) Electro- and (B) Photoelectrocatalytic Ethanol Oxidation

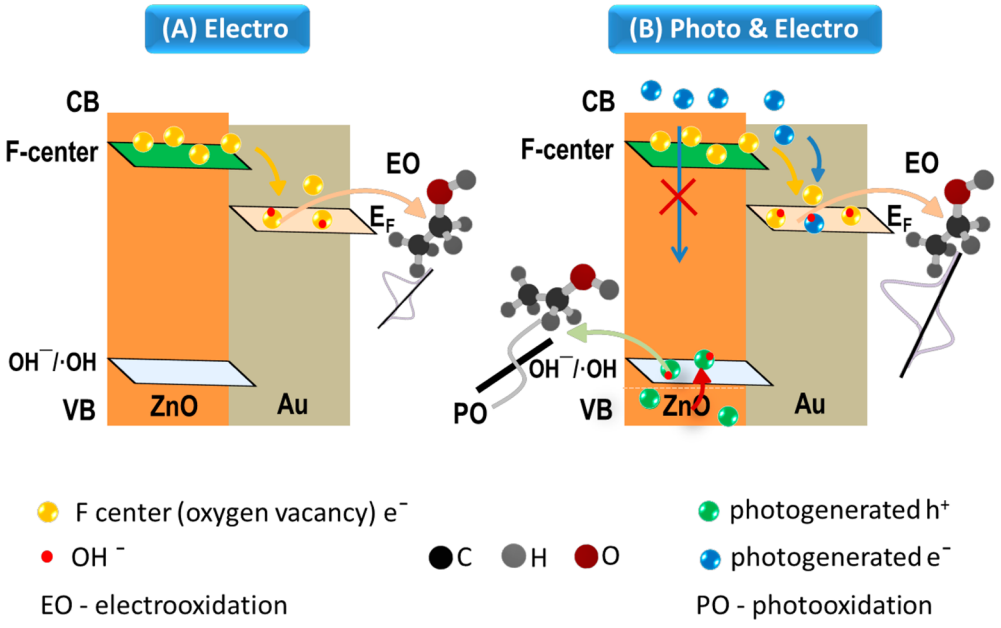

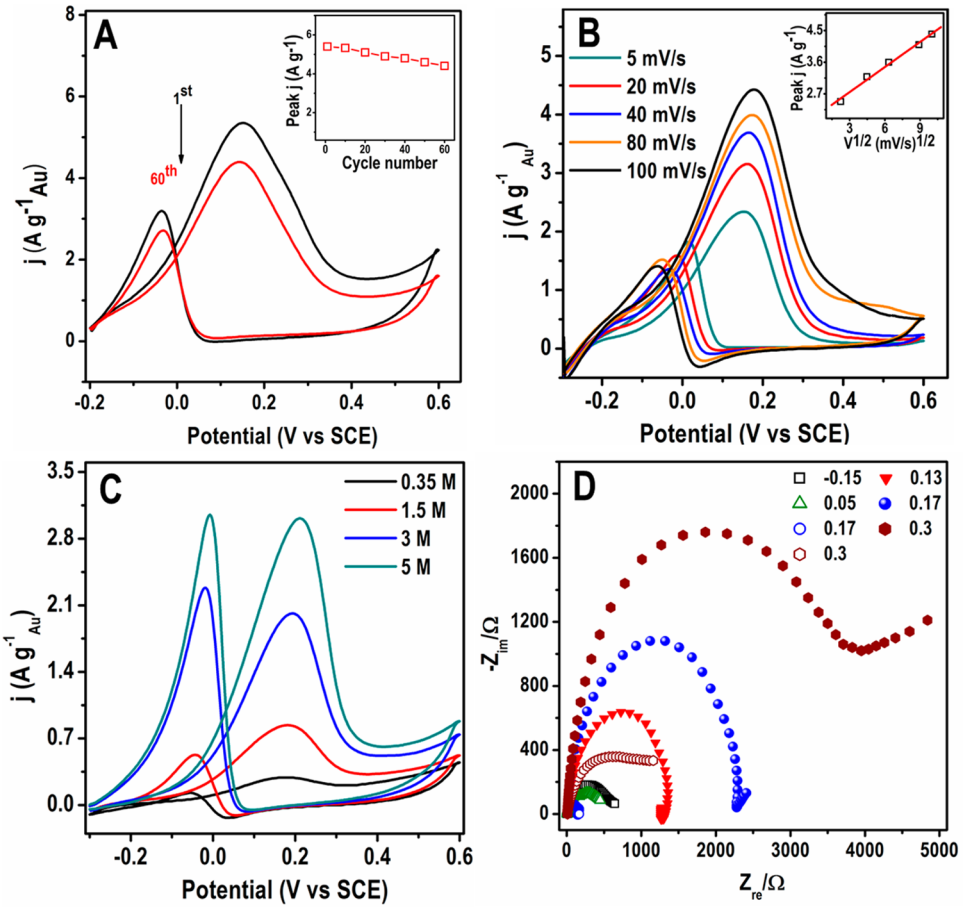

Figure 6. CV of mZnO/Au nanowires (A) stability test, in 5 M NaOH containing 2 M ethanol, first cycle and after 60th cycle; inset displays the peak current density versus cycle number at a scan rate of 10 mV/s, and (B) 3 M NaOH containing 1 M ethanol at different scan rates. Inset of (B) shows a linear relationship of current density with the square root of scan rate. (C) CVs at a scan rate of 40 mV/s in 1 M NaOH solutions with different concentrations of ethanol. (D) Electrochemical impedance spectra: Nyquist plot of the oxidation of ethanol over Au nanostructures supported on ZnO in 1 M NaOH and 1.5 M C_2H_5OH. The applied electrode potentials are shown as figure legends. Recorded from 100 kHz to 10 MHz with the amplitude of AC signal at 10 mV. Hollow and solid symbols are representative of mZnO/Au nanowires and ZnO/Au nanoparticles, respectively.

dx.doi.org/10.1021/ja5059444 | J. Am. Chem. Soc. 2014, 136, 14445−14455

a higher potential can lead to oxidation of the formed amine complex, thus favoring the formation of incipient hydrous oxide mediators on Au in the successive cycles. However, the amine layer oxidation destabilizes the nanowires significantly during reaction, resulting in the disintegration of the nanowires to nanoparticles (as shown in Figure 5C and D). Regardless of the morphological change, requirement of high potential to activate the gold surface is not viable for fuel cell applications.

The above results highlights that the formation of interfacial hydrous oxide mediators during the positive scan is different for unsupported and for ZnO supported Au nanowires. This finding is crucial because it implies that the mZnO support has an electronic effect that is important for the formation of hydrous gold oxide at low potential. To verify further the conjecture about the electronic effect induced by mZnO, we carried out detailed XPS studies on mZnO/Au (Figure 4D). We observe peaks at binding energy of 82.8 and 86.8 eV corresponding to Au $4f_{7/2}$ and $4f_{5/2}$ of $Au^{\delta-}$, respectively, and also a peak at 83.7 eV that can be rationalized by the presence of Au^0 state. The formation of $Au^{\delta-}$ indicates that there is electron transfer to Au from the substrate. This can happen in two ways. Recent investigations have shown that capping agents like OA could cause a change in the Au electronic structure by back-donating electron to Au nanostructures which can cause Au core level binding energy shift.[52] This possibility was discarded by an XPS study on unsupported OA capped nanowires that showed that Au^0 and small amount of $Au^{\delta+}$ are present in the system (Figure S13), indicating that a charge transfer between amine and Au may be insignificant in our system. The second possibility is the transfer of electrons from the ZnO to the Au. However, it may not be favorable to transfer electrons from the valence band of ZnO to Au. The presence of F-centers lead to the existence of electronic states located at 0.05 eV below the conduction band of ZnO that could favor electron transfer to Au (Scheme 1A).[53] According to work function levels, an electron from F-center of ZnO (4.4 eV) can migrate toward Au which has work function of 5 eV and can lead to electron-rich Au structures.[54−56]

According to the Norskov d-band model, the relatively deep d-band below Fermi energy is the primary reason for the inertness of gold toward chemisorption of oxygenated species.[57] It is well know that particle size reduction can shift the d-band state and reduce the barrier for chemisorption.[58] Alternatively, in the hybrid, a charge transfer from the F-center ZnO would better explain the upward shift of the Au Fermi level.[59] The increased electron density in Au would be beneficial for hydroxyl adsorption due to preferred electron donation from Au to highly electronegative adsorbates. For instance, Koper et al.[60] performed a detailed investigation regarding electrochemical oxidation of CO on Au in alkaline medium and proposed as "self-promotion mechanism" due to tendency to enhance adsorption of hydroxyl groups. In the present case, a consequence of the upward shift in Fermi level of Au enhances the adsorption of electronegative OH^- adsorbates, thereby driving the formation of hydrous oxide mediators on gold at very low potential. Thus, the ZnO support favors for the formation of incipient hydrous oxides on the gold surface that act as mediators for EOX; however, in the case of bare nanowires, repeated high positive potential cycling is needed to activate the gold surface to promote oxidation reactions.

To evaluate the long-term performance of the mZnO/Au nanowires, we carried out repeated scans with the same electrode. At the end of the 60 cycles, there is no significant decrease in oxidation current, indicating the stability of the hybrid (Figure 6A). The inset depicts that peak current density versus respective cycle number. In addition, we note that there is no significant change in the microstructure of the mZnO/Au hybrid after electrocatalysis (Figure S14). Our method of direct growth on the substrate thus overcomes the stability issues of nanowires in ethanol medium and thus opens up new possibilities for various potential applications.[14]

The impact of scan rate on the electrocatalytic performance on mZnO/Au, as shown in Figure 6B, shows that the current density is linearly proportional to the square root of scan rates (inset of Figure 6B). This is characteristic of a diffusion-controlled process limited by the diffusion of either ethanol or the reaction intermediates. Moreover, from Figure 6C, we observe that, upon increasing the ethanol concentration, oxidation current linearly increased and a subsequent decrease in gold oxide layer reduction cathodic current occurred. This can be rationalized due to ample availability of ethanol molecules to interact with formed gold oxide layer during initial period of electrochemical reduction process.[50]

To compare the role of the morphology of Au on the electrocatalytic activity, we compare the activity of mZnO/Au nanowires with the activity of ZnO/Au nanoparticles synthesized by microwave synthesis. Optical absorption and TEM micrographs of the synthesized Au nanoparticle hybrids are shown in Figure S10 and S15, respectively. The hybrid Au nanoparticles (Figure S16) displayed current density that is approximately 1.5 times lower than obtained with hybrid Au nanowires (Figure 4A). The mass specific current density of mZnO/Au nanowires shows a clear enhancement in activity in the case of nanowires. The possible reason for the higher activity of mZnO/Au nanowires can be attributed to the following geometric effects. First, 1D nanostructures that are single crystalline inherently possess less defects as compared to nanoparticles.[61] Generally, defect sites are irreversibly oxidized under applied potential that degrades the electrocatalytic performance. Second, diffusion of electrochemical species toward catalyst surfaces are significantly improved in high aspect ratio nanowires as has been demonstrated experimentally earlier.[62] Third, interconnected wires could also facilitate easier charge transport,[63] thus enhancing the electrocatalytic activity. Thus, the morphology of the Au on the ZnO support plays a key role in its electrocatalytic activity.

Electrochemical impedance spectroscopy (EIS) is a fundamental tool for characterizing the interfacial charge transfer properties of electrodes. Generally, the diameter of the semicircle in the Nyquist plot is equal to the charge transfer resistance (R_{ct}) of the electrode surface. Figure 6D indicates the representative complex plane of the Nyquist plot for synthesized hybrids in 1 M NaOH and 1.5 M ethanol at different applied potentials over the frequency range of 100 kHz to 10 mHz (with AC signal amplitude of 10 mV). It is found that ZnO/Au nanowires have a low R_{ct} value as compared to ZnO/Au nanoparticles, that is in accordance with the above results of CV. The calculated values of R_{ct} at 0.17 V are 130 Ω and 2.25 kΩ for mZnO/Au nanowires and ZnO/Au nanoparticles, respectively. The profiles indicate that R_{ct} decreases upon increasing the potential (from −0.15 to 0.17 V) and then increases at higher potential (0.3 V) for the nanowire hybrid. This is due to the formation of monolayer surface oxides at higher potential and consistent with the CV results.

dx.doi.org/10.1021/ja5059444 | J. Am. Chem. Soc. 2014, 136, 14445−14455

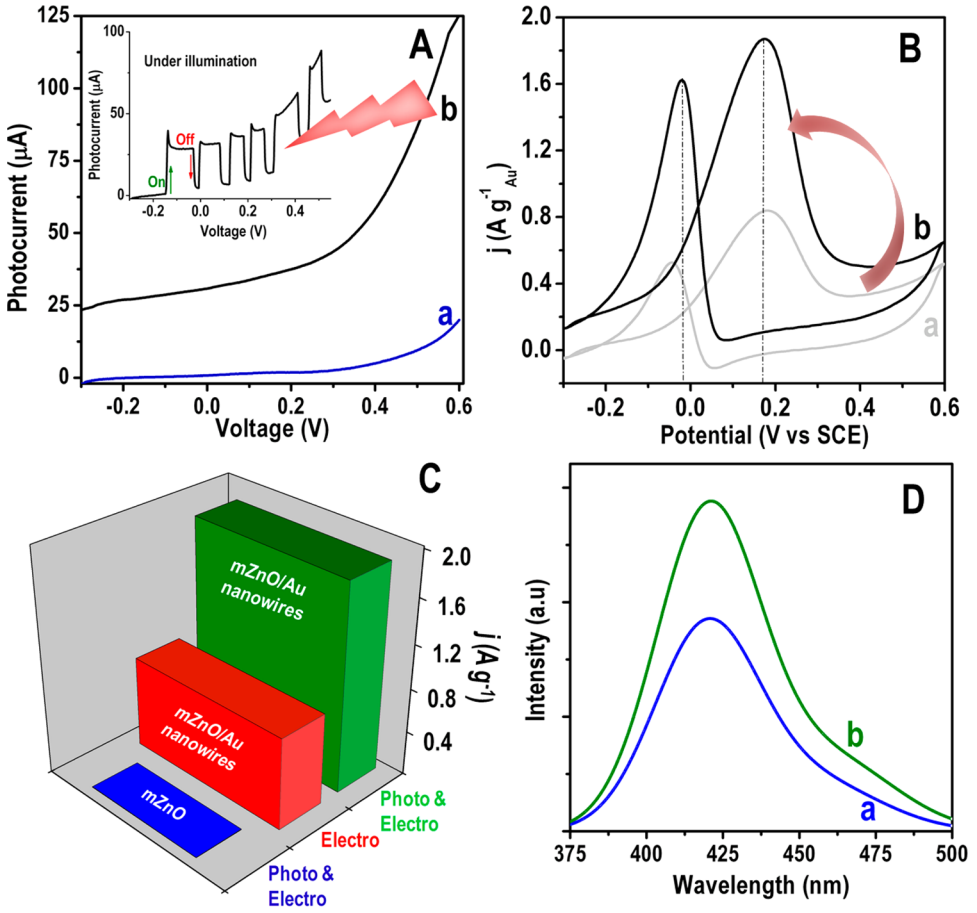

Figure 7. (A) Electrocurrent (a) and photocurrent (b) of mZnO electrode. Inset shows the ON/OFF switching photoresponse of mZnO electrode upon solar irradiation (xenon lamp). (B) CVs of mZnO/Au nanowires without (a) and with (b) solar light irradiation in 1 M NaOH containing 1.5 M ethanol. (C) Summary of the synergetic effect of photogenerated charge carrier on current density evaluated by CV measurements. (D) PL spectra of TAOH formed after 5 CV cycles of potential sweep from −0.3 to 0.6 V for the electrolyte (6 mM TA in 0.1 M NaOH) of the irradiated mZnO (a) and mZnO/Au nanowires (b) electrode at a scan rate of 40 mV/s.

Electrooxidation of ethanol did not take place with just mZnO as the catalyst that confirms that the observed electrocatalytic activity in the mZnO/Au hybrid primarily stems from the Au. However, upon irradiation, a substantial increase in current density was observed for mZnO at different applied potentials, as shown in Figure 7A. In the case of ZnO, the enhanced photoresponse at different potential is pronounced, leading to merging of EOX peak with generated photocurrent. It is understood that under illumination electron and hole pairs are created in ZnO (reaction 5). Typically, the photogenerated holes in alkaline medium are effectively scavenged by OH^- groups that protect the ZnO from dissolution, which leads to the formation of surface bound •OH[64] radicals (reaction 6) or direct oxidization of ethanol to form intermediate oxidized radical.

$$ZnO + h\nu \rightarrow e_{CB}^{-} + h_{VB}^{+} \quad (5)$$

$$ZnO{-}OH + h^{+} \rightarrow ZnO + \bullet OH \quad (6)$$

$$C_2H_5OH + \bullet OH \rightarrow \bullet CH(OH)CH_3 + H_2O \quad (7)$$

$$\bullet CH(OH)CH_3 + 11\bullet OH \rightarrow 2CO_2 + 8H_2O \quad (8)$$

The energy levels of intermediate (reaction 7) α-hydroxyethyl radicals •$CH(OH)CH_3$ are favorable for injecting an electron to conduction band of ZnO.[65,44] By combining the observed current increase and knowledge that we have gained from the studies with the proposed mechanism by the model of Morrison and Freund,[66] we are postulating that "current doubling" phenomenon occurs due to two step oxidation. Therefore, for single photon absorption, two electrons are injected into the conduction band, one by photoexcited electrons and other from intermediate radicals that leads to the increase in current. As shown earlier, Au nanowires are responsible for the observed electrocatalytic oxidation current in the synthesized mZnO/Au nanowires. We have demonstrated that mZnO also oxidizes ethanol under solar light and thus an effective coupling of these two processes (reaction 1 to 8) can boost the performance of the fuel cell.

Synergistic Photoelectrooxidation of Ethanol. The electrooxidation current response of the mZnO/Au nanowire hybrids under illumination is shown in Figure 7B. The characteristic EOX peak was shifted to lower onset potential under irradiation. Similarly, the oxidation of carbonate species that occurred during the reverse scan was shifted to more positive potential, as marked in the figure as dotted line. The reason for the reduced overpotential in the electrocatalytic reaction could arise from the enhanced hydrophilicity of photoinduced defect sites on ZnO,[67,68] which leads to increased concentration of ethanol on the active site of electrode surface.[27] Furthermore, the magnitude of the current density was enhanced by 2.2 times and is higher than the algebraic

dx.doi.org/10.1021/ja5059444 | J. Am. Chem. Soc. 2014, 136, 14445−14455

summation of photooxidation of mZnO and electrocatalytic activity of mZnO/Au nanowires as shown in Figure 7C. This is attributed to additional photooxidation and electrooxidation reactions of the formed byproduct acetic acid (reaction 4) and photogenerated electrons, respectively. This observation emphasizes the synergistic effect of photoassisted electrocatalytic activity, which intensifies the oxidation current.[28] Synergistic effect in the hybrid arises from efficient interfacial charge transfer and prominent separation of photogenerated holes and electrons. As the Fermi level of Au is lower than that of ZnO,[44] the photogenerated electron from conduction band of mZnO can migrate toward Au nanowires grown on mZnO leading to the net separation of photogenerated holes and electron pairs, as illustrated in Scheme 1B, which is consistent with observed photocurrent measurement. Subsequently, the photomigrated electrons further stimulate hydroxyl binding on Au nanowires that further enhance the electrocatalytic EOX (reaction 8), as seen above. The isolated holes can react with hydroxyl groups on the ZnO and produce an •OH radical that leads to photooxidation of ethanol (reaction 9).

$$CH_3CH_2OH + 5Au(OH^-) \rightarrow CH_3COO + 4H_2O + 4e^- \quad (8)$$

$$CH_3CH_2OH + 12\bullet OH(mZnO...OH + h^+) \rightarrow 2CO_2 + 9H_2O \quad (9)$$

The photogenerated charge separation efficiency of hybrid can be indirectly qualified by the amount of produced •OH radicals. Fluorescence measurement with terephthalic acid (TA) is employed to analyze the •OH radicals (Supporting Information). PL measurements (Figure 7D) give direct evidence for the formation of 2-hydroxyterephthalic acid as a result of interaction between terephthalic acid and produced •OH, resulting in PL emission around 422 nm (excited at 325 nm). The PL intensity increased for mZnO/Au nanowires as compared to mZnO as shown in Figure 7D, indicating enhanced separation of holes and electrons in mZnO/Au nanowires. These results highlight the direct consequence of separated photogenerated holes and electrons by interfacial charge migration between mZnO and Au nanowires. At the first step, the hybrid structure minimizes the recombination of photogenerated holes and electrons and thus enhances the production of •OH, which not only increases the photooxidation of ethanol but it can also participate in the photooxidization of the product formed during reaction 4. Meanwhile, the photomigrated electron induces negatively charged species in addition to F-center electrons around the Au surface, which increases the electrocatalytic activity via OH^- adsorption.

In summary, we have developed a method for the synthesis of high dense ultrathin Au wires on ZnO nanorods for electrocatalytic applications. Oleylamine modified ZnO shows an enhancement in the photocurrent by passivated surface defects. Support is mandatory to circumvent the disintegration of nanowires especially in ethanol medium. In addition to the stability, the support induces electronic effect on Au nanowires, which facilitates redox process at low potential. Considerably, high positive potential sweeps are needed to initiate the electrochemical reaction on unsupported oleylamine capped nanowires. These informative results are significant for understanding the key steps involved in the electrocatalytic activity of surfactant capped nanostructures. Most importantly, it was revealed that hybrids upon photoirradiation accelerate the activity of Au, by interfacial migration of photoelectron which suppresses the recombination of photogenerated carriers thus leading to synergy between electro and photooxidation current. Although the scope of this work is limited to fuel cell, interfacing ultrathin nanowire with semiconductor can enhance various physic-chemical properties. We believe that the research community will leverage the synthesized nanowire hybrids for many exciting applications in the fields of nanoelectronics, sensors, and catalysis.

EXPERIMENTAL SECTION

Synthesis of ZnO Nanorods. ZnO nanorods (~1 μm length) were synthesized according to our earlier report. Zinc acetate (14.5 g) was dissolved in 62.5 mL of methanol, and then KOH (4 M, 32.5 mL methanol) was added to the above solution under vigorous stirring at 67 °C. After the mixture was aged for 2 h to evaporate half the volume of solvent, the concentrated solution was incubated in a stainless steel autoclave for 12 h at 120 °C. Finally, the obtained product was washed several times with distilled water and dried at 100 °C.

Oleylamine (OA) Modified ZnO (mZnO). ZnO was passivated with oleylamine by means of simple solid state reaction. In a typical synthesis, 100 mg of ZnO nanorods was taken in a mortar and mixed with 50 μL of OA using a pestle at room temperature that resulted in the formation of amine grafted ZnO. The product was repeatedly washed with hexane and ethanol mixture to remove unbound OA and then dried in ambient conditions.

Preparation of mZnO/Au Nanowires. To produce the hybrid material, as prepared mZnO (10 mg), 3 mg of $HAuCl_4$, 100 μL of OA, and 150 μL of triisopropylsilane(TIPS) were added into 2.5 mL of hexane following the method of Xing et al.[15] The mixture was sonicated for 2 min and then kept without stirring for 6 h until the color of the solution changed to dark red. The obtained precipitate was washed thrice with an ethanol/hexane mixture using centrifugation, and the final products were used for further photo- and electrocatalytic study.

Preparation of ZnO/Au Nanoparticles. ZnO/Au nanoparticles were prepared through a microwave assisted synthesis route, according to our previous study.[30] An amount of 50 mg of synthesized ZnO nanorods was sonicated in 30 mL of water for 10 min, followed by the addition of $HAuCl_4$ (3 mg). This was subject to microwave radiation (2.45 GHz, 800 W) for 3 min to obtain ZnO/Au nanoparticles hybrid.

Characterizations. TEM micrographs were acquired using a FEI Tecnai T20 instrument operated at an accelerating voltage of 200 kV, and HAADF images were obtained using a FEI Tecnai T30 instrument with an accelerating voltage of 300 kV. XPS measurements were performed on an Axis Ultra instrument using a monochromatic source of Al Kα radiation, and charge correction was done with respect to graphitic carbon at 284.5 eV. FT-IR spectra were recorded using a UATR accessory on a Frontier PerkinElmer spectrometer. The composition quantification of Au was found using inductively coupled plasma-mass spectroscopy (ICP-MS, Thermo X Series II). Photoluminescence spectra for both solid catalyst and liquid electrolyte samples were measured using a LabRAM HR spectrophotometer with the help of a CCD detector.

Photoconductivity Measurements. Photocurrent measurements were done using a Class 3A solar simulator (Oriel Sol 3A) comprising a xenon lamp 450 W, with a 1.5 air mass filter and a Keithley (2420 model) source meter. The samples were drop casted between ITO contact pads coated on glass and separated at a distance of 50 μm. The electrical measurements were performed using an Agilent Device analyzer B1500A.

Photoelectrochemical Measurements. A conventional three electrode system was adopted to perform cyclic voltammetry experiments using saturated calomel electrode (SCE) and platinum foil auxiliary as reference and counter electrode, respectively. The working electrode of nanowire hybrids was fabricated by loading hexane dispersed hybrids on toray carbon paper. The catalyst ink of

dx.doi.org/10.1021/ja5059444 | J. Am. Chem. Soc. 2014, 136, 14445−14455

nanoparticle hybrids was made by mixing 15 mg of nanoparticle hybrid with 30 μL of Nafion in isopropanol solvent, and then the prepared ink was drop casted on toray paper. CVs of the prepared electrodes were measured with and without light irradiation. A xenon lamp of 100 W was employed as an excitation source. All the electrochemical measurements were conducted at room temperature and performed by using a potentiostat (PG26250, Techno Science Instrument).

Electrochemical Impedance Spectroscopy (EIS) Measurements. EIS was performed using a CHI 660D electrochemical workstation. The spectra were recorded from 100 kHz to 10 MHz at an AC signal of 10 mV.

■ ASSOCIATED CONTENT

Supporting Information

Procedure for terephthalic test and ECSA calculation. Figures S1−S16. This material is available free of charge via the Internet at http://pubs.acs.org.

■ AUTHOR INFORMATION

Corresponding Author

nravi@mrc.iisc.ernet.in

Notes

The authors declare no competing financial interest.

■ ACKNOWLEDGMENTS

We thank Prof. Praveen C. Ramamurthy for providing chemical workstation facilities for impedance measurements. The authors thank Prof. Ramananda Chakrabarti and his students for access to the ICP-MS facility. The Tecnai T20 and F30 microscopes are part of Advanced facility for Microscopy and Microanalysis at IISc. The XPS, solar simulator, and PL spectrophotometer are part of MNCF, CeNSE, IISc. The authors thank Subhajit Kundu and Akash for their help with TEM imaging. N.R. thanks DST Nanomission and TUE, DST for financial support.

■ REFERENCES

(1) Kowal, A.; Li, M.; Shao, M.; Sasaki, K.; Vukmirovic, M.; Zhang, J.; Marinkovic, N.; Liu, P.; Frenkel, A.; Adzic, R. *Nat. Mater.* **2009**, *8*, 325−330.

(2) Antolini, E. *J. Power Sources* **2007**, *170*, 1−12.

(3) He, Q.; Shyam, B.; Macounová, K.; Krtil, P.; Ramaker, D.; Mukerjee, S. *J. Am. Chem. Soc.* **2012**, *134*, 8655−8661.

(4) Beden, B.; Lamy, C.; De Tacconi, N.; Arvia, A. *Electrochim. Acta* **1990**, *35*, 691−704.

(5) Wang, A.-L.; Xu, H.; Feng, J.-X.; Ding, L.-X.; Tong, Y.-X.; Li, G.-R. *J. Am. Chem. Soc.* **2013**, *135*, 10703−10709.

(6) Xu, C.; Wang, H.; Shen, P. K.; Jiang, S. P. *Adv. Mater.* **2007**, *19*, 4256−4259.

(7) Tian, N.; Zhou, Z.-Y.; Yu, N.-F.; Wang, L.-Y.; Sun, S.-G. *J. Am. Chem. Soc.* **2010**, *132*, 7580−7581.

(8) Koenigsmann, C.; Santulli, A. C.; Gong, K.; Vukmirovic, M. B.; Zhou, W.-p.; Sutter, E.; Wong, S. S.; Adzic, R. R. *J. Am. Chem. Soc.* **2011**, *133*, 9783−9795.

(9) Lu, Y.; Tu, J.-p.; Gu, C.-d.; Xia, X.-h.; Wang, X.-l.; Mao, S. X. *J. Mater. Chem.* **2011**, *21*, 4843−4849.

(10) Ruan, L.; Zhu, E.; Chen, Y.; Lin, Z.; Huang, X.; Duan, X.; Huang, Y. *Angew. Chem., Int. Ed.* **2013**, *52*, 12577−12581.

(11) Koenigsmann, C.; Sutter, E.; Adzic, R. R.; Wong, S. S. *J. Phys. Chem. C* **2012**, *116*, 15297−15306.

(12) Kondo, Y.; Takayanagi, K. *Science* **2000**, *289*, 606−608.

(13) An, W.; Pei, Y.; Zeng, X. *Nano Lett.* **2008**, *8*, 195−202.

(14) Koposova, E.; Kisner, A.; Shumilova, G.; Ermolenko, Y.; Offenhäusser, A.; Mourzina, Y. *J. Phys. Chem. C* **2013**, *117*, 13944−13951.

(15) Feng, H.; Yang, Y.; You, Y.; Li, G.; Guo, J.; Yu, T.; Shen, Z.; Wu, T.; Xing, B. *Chem. Commun.* **2009**, 1984−1986.

(16) Choi, Y.; Gu, M.; Park, J.; Song, H. K.; Kim, B. S. *Adv. Energy Mater.* **2012**, *2*, 1510−1518.

(17) Cui, H.; Hong, C.; Ying, A.; Yang, X.; Ren, S. *ACS Nano* **2013**, *7*, 7805−7811.

(18) Chandni, U.; Kundu, P.; Singh, A. K.; Ravishankar, N.; Ghosh, A. *ACS Nano* **2011**, *5*, 8398−8403.

(19) Kundu, P.; Chandni, U.; Ghosh, A.; Ravishankar, N. *Nanoscale* **2012**, *4*, 433−437.

(20) Halder, A.; Ravishankar, N. *Adv. Mater.* **2007**, *19*, 1854−1858.

(21) Kundu, P.; Anumol, E.; Nethravathi, C.; Ravishankar, N. *Phys. Chem. Chem. Phys.* **2011**, *13*, 19256−19269.

(22) Kulesza, P. J.; Pieta, I. S.; Rutkowska, I. A.; Wadas, A.; Marks, D.; Klak, K.; Stobinski, L.; Cox, J. A. *Electrochim. Acta* **2013**, *110*, 474−483.

(23) Liu, B.; Chia, Z.-W.; Lee, Z.-Y.; Cheng, C.-H.; Lee, J.-Y.; Liu, Z.-L. *J. Power Sources* **2012**, *206*, 97−102.

(24) Li, W.; Bai, Y.; Li, F.; Liu, C.; Chan, K.-Y.; Feng, X.; Lu, X. *J. Mater. Chem.* **2012**, *22*, 4025−4031.

(25) Georgieva, J.; Valova, E.; Armyanov, S.; Philippidis, N.; Poulios, I.; Sotiropoulos, S. *J. Hazard. Mater.* **2012**, *211*, 30−46.

(26) Antoniadou, M.; Lianos, P. *Appl. Catal., B* **2010**, *99*, 307−313.

(27) Su, C.-Y.; Hsueh, Y.-C.; Kei, C.-C.; Lin, C.-T.; Perng, T.-P. *J. Phys. Chem. C* **2013**, *117*, 11610−11618.

(28) Drew, K.; Girishkumar, G.; Vinodgopal, K.; Kamat, P. V. *J. Phys. Chem. B* **2005**, *109*, 11851−11857.

(29) Tian, Z. R.; Voigt, J. A.; Liu, J.; Mckenzie, B.; Mcdermott, M. J.; Rodriguez, M. A.; Konishi, H.; Xu, H. *Nat. Mater.* **2003**, *2*, 821−826.

(30) Leelavathi, A.; Madras, G.; Ravishankar, N. *Phys. Chem. Chem. Phys.* **2013**, *15*, 10795−10802.

(31) Koleilat, G. I.; Levina, L.; Shukla, H.; Myrskog, S. H.; Hinds, S.; Pattantyus-Abraham, A. G.; Sargent, E. H. *ACS Nano* **2008**, *2*, 833−840.

(32) Lan, X.; Masala, S.; Sargent, E. H. *Nat. Mater.* **2014**, *13*, 233−240.

(33) Tang, J.; Kemp, K. W.; Hoogland, S.; Jeong, K. S.; Liu, H.; Levina, L.; Furukawa, M.; Wang, X.; Debnath, R.; Cha, D. *Nat. Mater.* **2011**, *10*, 765−771.

(34) Mourdikoudis, S.; Liz-Marzán, L. M. *Chem. Mater.* **2013**, *25*, 1465−1476.

(35) Kundu, P.; Halder, A.; Viswanath, B.; Kundu, D.; Ramanath, G.; Ravishankar, N. *J. Am. Chem. Soc.* **2009**, *132*, 20−21.

(36) Loubat, A.; Impéror-Clerc, M.; Pansu, B.; Meneau, F.; Raquet, B.; Viau, G.; Lacroix, L.-M. *Langmuir* **2014**, *30*, 4005−4012.

(37) Kumar, D. R.; Manoj, D.; Santhanalakshmi, J. *Anal. Methods* **2014**, *6*, 1011−1020.

(38) Belagodu, T.; Azhar, E. A.; Yu, H. *Nanoscale* **2012**, *4*, 7330−7333.

(39) Soares, J. W.; Whitten, J. E.; Oblas, D. W.; Steeves, D. M. *Langmuir* **2008**, *24*, 371−374.

(40) Wang, J.; Liu, P.; Fu, X.; Li, Z.; Han, W.; Wang, X. *Langmuir* **2008**, *25*, 1218−1223.

(41) Guo, L.; Yang, S.; Yang, C.; Yu, P.; Wang, J.; Ge, W.; Wong, G. K. *Chem. Mater.* **2000**, *12*, 2268−2274.

(42) Yang, W.; Qu, L.; Zheng, R.; Liu, Z.; Ratinac, K. R.; Shen, L.; Yu, D.; Yang, L.; J. Barrow, C.; Ringer, S. P.; Dai, L.; Braet, F. *Chem. Mater.* **2011**, *23*, 2760−2765.

(43) Wang, C.; Hu, Y.; Lieber, C. M.; Sun, S. *J. Am. Chem. Soc.* **2008**, *130*, 8902−8903.

(44) Subramanian, V.; Wolf, E. E.; Kamat, P. V. *J. Phys. Chem. B* **2003**, *107*, 7479−7485.

(45) Yan, S.; Zhang, S.; Lin, Y.; Liu, G. *J. Phys. Chem. C* **2011**, *115*, 6986−6993.

(46) Lai, S.; Kleijn, S. E.; Öztürk, F. T.; van Rees Vellinga, V. C.; Koning, J.; Rodriguez, P.; Koper, M. *Catal. Today* **2010**, *154*, 92−104.

(47) Huang, J.; Han, X.; Wang, D.; Liu, D.; You, T. *ACS Appl. Mater. Interfaces* **2013**, *5*, 9148−9154.

(48) Burke, L.; Nugent, P. *Gold Bull.* **1998**, *31*, 39−50.

(49) Zope, B. N.; Hibbitts, D. D.; Neurock, M.; Davis, R. J. *Science* **2010**, *330*, 74−78.

(50) De Lima, R.; Varela, H. *Gold Bull.* **2008**, *41*, 15−22.
(51) Tremiliosi-Filho, G.; Gonzalez, E.; Motheo, A.; Belgsir, E.; Léger, J.-M.; Lamy, C. *J. Electroanal. Chem.* **1998**, *444*, 31−39.
(52) Zhang, G.-R.; Xu, B.-Q. *Nanoscale* **2010**, *2*, 2798−2804.
(53) Schmidt-Mende, L.; MacManus-Driscoll, J. L. *Mater. Today* **2007**, *10*, 40−48.
(54) Wang, J.; Hammer, B. *Top. Catal.* **2007**, *44*, 49−56.
(55) Radnik, J.; Mohr, C.; Claus, P. *Phys. Chem. Chem. Phys.* **2003**, *5*, 172−177.
(56) Arrii, S.; Morfin, F.; Renouprez, A.; Rousset, J. *J. Am. Chem. Soc.* **2004**, *126*, 1199−1205.
(57) Hammer, B.; Norskov, J. *Nature* **1995**, *376*, 238−240.
(58) Lopez, N.; Janssens, T.; Clausen, B.; Xu, Y.; Mavrikakis, M.; Bligaard, T.; Nørskov, J. K. *J. Catal.* **2004**, *223*, 232−235.
(59) Sanchez, A.; Abbet, S.; Heiz, U.; Schneider, W.-D.; Häkkinen, H.; Barnett, R.; Landman, U. *J. Phys. Chem. A* **1999**, *103*, 9573−9578.
(60) Rodriguez, P.; Kwon, Y.; Koper, M. T. *Nat. Chem.* **2012**, *4*, 177−182.
(61) Koenigsmann, C.; Zhou, W.-p.; Adzic, R. R.; Sutter, E.; Wong, S. S. *Nano Lett.* **2010**, *10*, 2806−2811.
(62) Wu, P.; Zhang, H.; Qian, Y.; Hu, Y.; Zhang, H.; Cai, C. *J. Phys. Chem. C* **2013**, *117*, 19091−19100.
(63) Sánchez-Iglesias, A.; Rivas-Murias, B.; Grzelczak, M.; Pérez-Juste, J.; Liz-Marzán, L. M.; Rivadulla, F.; Correa-Duarte, M. A. *Nano Lett.* **2012**, *12*, 6066−6070.
(64) Fujishima, A.; Kato, T.; Maekawa, E.; Honda, K. *Bull. Chem. Soc. Jpn.* **1981**, *54*, 1671−1674.
(65) Lu, H.; Zhao, J.; Li, L.; Gong, L.; Zheng, J.; Zhang, L.; Wang, Z.; Zhang, J.; Zhu, Z. *Energy Environ. Sci.* **2011**, *4*, 3384−3388.
(66) Morrison, S. R.; Freund, T. *J. Chem. Phys.* **1967**, *47*, 1543−1551.
(67) Feng, X.; Feng, L.; Jin, M.; Zhai, J.; Jiang, L.; Zhu, D. *J. Am. Chem. Soc.* **2004**, *126*, 62−63.
(68) Sun, R.-D.; Nakajima, A.; Fujishima, A.; Watanabe, T.; Hashimoto, K. *J. Phys. Chem. B* **2001**, *105*, 1984−1990.